# Interaction of the Near-Zone Fields of a Slot on a Conducting Sphere with a Spherical Model of Man

SHI-GUO ZHU, KUN-MU CHEN, FELLOW, IEEE, AND HUEY-RU CHUANG, STUDENT MEMBER, IEEE

*Abstract*—**We consider the geometry of a lossy dielectric sphere, simulating a human body, placed in the proximity of a conducting sphere with a radiating slot, simulating a leaking microwave oven. An exact solution is obtained for this idealized problem by using two spherical coordinate systems and employing the addition theorem to translate the vector spherical harmonics between the coordinate systems. Multiple scatterings of the EM wave between the two spheres are determined by solving the boundary value problems iteratively. An extensive numerical computation has been conducted to determine the induced SAR in the dielectric sphere, and the body–source coupling effect was evaluated. It was found that a serious error in the SAR estimation can be caused if the body–source coupling is neglected, a common approximation used in most of the existing studies on the subject.**

## I. Introduction

IN RECENT YEARS, due to the widespread use of microwave radiation in medical, industrial, and household applications, and to the controversy over its potential adverse health effect, studies of the interaction of microwave radiation with the human body have developed into a scientific field called bioelectromagnetics. In the field of bioelectromagnetics, one of the important subjects is dosimetry. This subject deals with theoretical predictions and experimental measurements of the induced electromagnetic (EM) field in the biological body excited by a known impressed EM field or a given EM source.

Numerous studies [1]–[4] have been conducted to predict the induced EM field in biological bodies when they are irradiated by the far-zone EM field or a plane EM wave. These studies contributed to an understanding of the coupling of EM energy into the human body and also led to the modification of the nonionizing radiation safety standards.

Unfortunately, in most of the medical, industrial, and household applications of microwave radiation, the human body is exposed to the near-zone field of an EM source. One most common situation is the human body exposed to the potential leakage field of a microwave oven. Since the nature of a near-zone EM field is different from that of a far-zone EM field, and since the body–source coupling may become important when the body is located close to the EM source, knowledge of the interaction of the far-zone EM field with a human body may not be applicable to the case of the interaction of the near-zone EM field with a human body.

Recently, a number of studies [5]–[9] on the interaction of the near-zone EM field with biological bodies have been conducted. In all of these studies, the important body–source coupling effect has been neglected for the sake of simplicity. This neglecting of the body–source coupling, however, raises the question of the accuracy of those theoretical predictions. In a study [10] conducted by our group on the coupling between a dipole antenna and a human body, a significant body–source coupling was found. The purpose of the study was to examine carefully the nature of the interaction between the near-zone field of an aperture EM source on a conducting structure and a human body in the proximity. Through this study, the importance of the body–source coupling will be evaluated for this type of EM source.

One of the simplest geometries for an aperture EM source is a radiating slot on a conducting sphere. If this source geometry is combined with a spherical model of man, an exact solution can be obtained to predict the interaction of the near-zone field of an aperture EM source with the human body. This geometry can also simulate the situation of a human body exposed to the leakage field of a microwave oven.

In the present study, we adopt the geometry of a lossy dielectric sphere (simulating a human body) placed in the proximity of a conducting sphere (simulating a microwave oven) with a radiating slot (simulating a leakage gap). The induced EM field inside the dielectric sphere and the scattered EM field surrounding the conducting and the dielectric sphere maintained by the radiating slot were determined. Fortunately, for this geometry, an exact solution could be obtained. An exact solution was sought because only through such a solution could the body–source coupling effect be accurately estimated.

To solve this problem, two spherical coordinate systems were used to describe the conducting sphere (source) and the dielectric sphere (body). The EM fields were expressed in terms of vector spherical harmonics and the addition theorem was used to translate the EM fields between these two coordinate systems. Multiple scatterings of the EM

Manuscript received October 12, 1983; revised March 9, 1984. This work was supported in part by the National Science Foundation under Grant ESC-8001772.

The authors are with the Department of Electrical Engineering and System Science, Michigan State University, East Lansing, MI 48824.

0018-9480/84/0800-0784$01.00 ©1984 IEEE

wave between the conducting sphere and the dielectric sphere were determined by solving the boundary value problems iteratively. Final solutions of the EM fields were obtained when the results of multiple scatterings converge. An extensive numerical computation was conducted to calculate the induced field inside the dielectric sphere. The body–source effect was evaluated numerically. It was found that more than 50-percent error in the estimation of the SAR in the body can be caused if the body–source coupling is neglected.

## II. Geometry of the Problem

The geometry of the problem is shown in Fig. 1. A perfectly conducting sphere of radius $a$ with a narrow radiating slot on its surface is described by a unprimed coordinate system (0 system). A lossy dielectric sphere of radius $b$ placed in the proximity of the conducting sphere is described by a primed coordinate system ($0'$ system). These two spheres are located in free space and their centers are separated by a distance of $r_0$. The polar axes, the $z$ and the $z'$ axis, of these two coordinate systems coincide. The radiating slot is located on the surface of the conducting sphere at $r = a$, $\theta = \theta_0$, and $-\alpha \leqslant \phi \leqslant \alpha$, as described in the 0 system. The dielectric sphere is assumed to be homogeneous and possesses permittivity $\epsilon$, conductivity $\sigma$, and permeability $\mu_0$ (free-space permeability).

This idealized geometry was adopted because it was simple enough to yield an exact solution and yet simulated the practical situation of a human body interacting with the near-zone leakage field of a microwave oven. An exact solution was needed because only an exact solution could lead to an accurate estimate of the coupling effect between the body and the source, the conducting sphere.

## III. Development of the Theory

The approach used in analyzing this problem is explained in Fig. 2. The final objective was to calculate the total induced field inside the dielectric sphere, and to achieve this goal the picture of multiple scatterings of the EM wave between these two spheres was employed. In the analysis, the addition theorem for the vector spherical harmonics played the key role in translating the vector spherical harmonics between the two coordinate systems.

As indicated in Fig. 2, the first step was to determine the near-zone field $[\vec{E}^{r(0)}, \vec{H}^{r(0)}]$ maintained by the slot in terms of vector spherical harmonics in unprimed coordinates $(r, \theta, \phi)$. The second step was to translate $[\vec{E}^{r(0)}, \vec{H}^{r(0)}]$ into primed coordinates $(r', \theta', \phi')$, using the addition theorem, to give the first-order incident field $[\vec{E}'^{i(1)}, \vec{H}'^{i(1)}]$ to the dielectric sphere. Note that the prime in the superscripts of fields indicates that the fields are expressed in terms of primed coordinates. The third step was to determine the first-order scattered field $[\vec{E}'^{s(1)}, \vec{H}'^{s(1)}]$ by the dielectric sphere and the first-order transmitted field $[\vec{E}'^{t(1)}, \vec{H}'^{t(1)}]$ in the dielectric sphere by solving the boundary value problem on the surface of the dielectric sphere. The fourth step was to translate the first-order scattered field $[\vec{E}'^{s(1)}, \vec{H}'^{s(1)}]$ by the dielectric sphere into

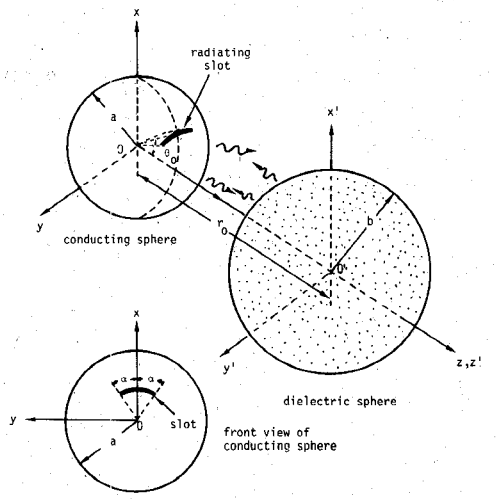


Fig. 1. A lossy dielectric sphere in the proximity of a conducting sphere with a radiating slot.

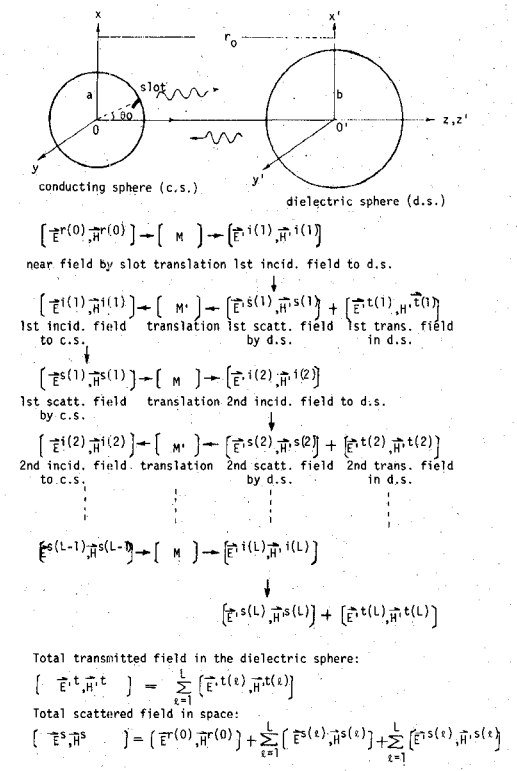


Fig. 2. Scattered and transmitted fields created by the multiple scattering of an EM wave of a radiating slot between a conducting and a lossy dielectric sphere.

unprimed coordinates $(r, \theta, \phi)$ to give the first-order incident field $[\vec{E}^{i(1)}, \vec{H}^{i(1)}]$ on the conducting sphere. The fifth step was to determine the first-order scattered field $[\vec{E}^{s(1)}, \vec{H}^{s(1)}]$ by the conducting sphere based on the boundary condition on the surface of the conducting sphere. The sixth step was to translate the first-order scattered field $[\vec{E}^{s(1)}, \vec{H}^{s(1)}]$ by the conducting sphere back to the primed coordinate system $(r', \theta', \phi')$ to give the second-order incident field $[\vec{E}'^{i(2)}, \vec{H}'^{i(2)}]$ to the dielectric sphere. Subsequently, the procedure of the third to the sixth step was repeated until the sums of multiple partial fields converged.

The total induced field inside the dielectric sphere is then the sum of the multiple partial transmitted fields $[\vec{E}^{t(l)}, \vec{H}^{t(l)}]$ in the dielectric sphere. The total scattered field surrounding the two spheres can be obtained by summing up the initial near-zone field $[\vec{E}^{r(0)}, \vec{H}^{r(0)}]$ of the slot and all the multiple partial scattered fields $[\vec{E}^{s(l)}, \vec{H}^{s(l)}]$ by the two spheres.

In the following sections, details of the development of the theory are given.

### A. Near-Zone Field Maintained by the Slot

The slot on the perfectly conducting sphere was assumed to have an aperture field given by

$$\vec{E}_a(a,\theta,\phi) = \begin{cases} \hat{\theta}\dfrac{1}{a}\delta(\theta-\theta_0)\cos(\pi\phi/2\alpha), & \text{for } -\alpha \leqslant \phi \leqslant \alpha \\ 0, & \text{elsewhere on } r=a \end{cases} \tag{1}$$

$\vec{E}_a$ is a cosinusoidal function of $\phi$ and it vanishes at the ends of the slot. It also implies a potential difference of 1 V across the slot at its center.

The EM field maintained by the slot aperture field at any point in space can be expressed in terms of vector spherical harmonics [11]. Thus, the near-zone field $[\vec{E}^{r(0)}, \vec{H}^{r(0)}]$ of the slot can be written as

$$\vec{E}^{r(0)}(r,\theta,\phi) = \sum_{n=0}^{\infty}\sum_{m=-n}^{n}\left[A_{mn}^{r(0)}\vec{M}_{mn}^{h}(r,\theta,\phi) + B_{mn}^{r(0)}\vec{N}_{mn}^{h}(r,\theta,\phi)\right] \tag{2}$$

$$\vec{H}^{r(0)}(r,\theta,\phi) = \frac{j}{\eta_0}\sum_{n=0}^{\infty}\sum_{m=-n}^{n}\left[B_{mn}^{r(0)}\vec{M}_{mn}^{h}(r,\theta,\phi) + A_{mn}^{r(0)}\vec{N}_{mn}^{h}(r,\theta,\phi)\right] \tag{3}$$

where the vector spherical harmonics $\vec{M}_{mn}$ and $\vec{N}_{mn}$ are given as

$$\vec{M}_{mn}(r,\theta,\phi) = \hat{\theta}\left[z_n(kr)\frac{jm}{\sin\theta}P_n^m(\cos\theta)e^{jm\phi}\right] - \hat{\phi}\left[z_n(kr)\frac{d}{d\theta}P_n^m(\cos\theta)e^{jm\phi}\right] \tag{4}$$

$$\vec{N}_{mn}(r,\theta,\phi) = \hat{r}\left[\frac{1}{kr}z_n(kr)n(n+1)P_n^m(\cos\theta)e^{jm\phi}\right] + \hat{\theta}\left\{\frac{1}{kr}\frac{d}{dr}[rz_n(kr)]\frac{d}{d\theta}P_n^m(\cos\theta)e^{jm\phi}\right\} + \hat{\phi}\left\{\frac{1}{kr}\frac{d}{dr}[rz_n(kr)]\frac{jm}{\sin\theta}P_n^m(\cos\theta)e^{jm\phi}\right\}. \tag{5}$$

In (4) and (5), $z_n(kr)$ represents any kind of spherical Bessel function of order $n$. The selection of $z_n(kr)$ depends on the nature of the field and whether or not the origin of the coordinate system is included. In our analysis, two kinds of $z_n(kr)$ were used; the first kind of spherical Bessel function $j_n(kr)$ implied an incoming wave, and the second kind of spherical Henkel function $h_n^{(2)}(kr)$ implied an outgoing wave. For example, the superscript $h$ for $\vec{M}_{mn}^{h}$ and $\vec{N}_{mn}^{h}$ in (2) and (3) indicates that $h_n^{(2)}(kr)$ was adapted for $z_n(kr)$. Similarly, when the superscript $j$ is used for $\vec{M}_{mn}^{j}$ and $\vec{N}_{mn}^{j}$, it means that $j_n(kr)$ was adapted for $z_n(kr)$. The propagation constant $k$ appearing in the expressions of $\vec{M}_{mn}$ and $\vec{N}_{mn}$ takes the value of $k_0 = \omega\sqrt{\mu_0\epsilon_0}$ for the scattered fields in space and the value of $k_d = \omega\sqrt{\mu_0\epsilon}\sqrt{1-j\sigma/\omega\epsilon}$ for the transmitted fields in the dielectric sphere. $P_n^m(\cos\theta)$ is the associated Legendre function of order $n$ and degree $m$. $\eta_0$ is the impedance of free space and is equal to $\sqrt{\mu_0/\epsilon_0}$. The coefficients $A_{mn}^{r(0)}$ and $B_{mn}^{r(0)}$ associated with $\vec{M}_{mn}^{h}$ and $\vec{N}_{mn}^{h}$ in (2) and (3) are to be determined by matching the field on the surface of the conducting sphere.

It is noted that, in the derivation of (3), the following relations were used:

$$\nabla\times\vec{E}^{r(0)} = -j\omega\mu_0\vec{H}^{r(0)}$$

$$\vec{N}_{nm} = \frac{1}{k}\nabla\times\vec{M}_{mn}, \quad \vec{M}_{mn} = \frac{1}{k}\nabla\times\vec{N}_{mn}$$

$$\vec{M}_{mn} = \vec{N}_{mn} = 0, \quad \text{for } m=n=0.$$

If the electric $\vec{E}^{r(0)}(a,\theta,\phi)$ given in (2) is matched to the slot aperture field $\vec{E}_a(a,\theta,\phi)$ given in (1) on the surface of the conducting sphere at $r=a$, the following equation is obtained:

$$\sum_{n=0}^{\infty}\sum_{m=-n}^{n}\left[A_{mn}^{r(0)}\vec{M}_{mn}^{h}(a,\theta,\phi) + B_{mn}^{r(0)}\vec{N}_{mn}^{h}(a,\theta,\phi)\right] = \begin{cases} \hat{\theta}\dfrac{1}{a}\delta(\theta-\theta_0)\cos(\pi\phi/2\alpha), & \text{for } -\alpha\leqslant\phi\leqslant\alpha \\ 0, & \text{elsewhere} \end{cases} \tag{6}$$

The coefficients $A_{mn}^{r(0)}$ and $B_{mn}^{r(0)}$ can then be determined using the orthogonal properties of vector spherical harmonics to be

$$A_{mn}^{r(0)} = -j\frac{m\alpha\cos m\alpha}{a(\pi^2-4m^2\alpha^2)}\frac{(2n+1)}{(1+\delta_m)n(n+1)}\cdot\frac{(n-m)!}{(n+m)!}\frac{P_n^m(\cos\theta_0)}{h_n^{(2)}(k_0a)} \tag{7}$$

$$B_{mn}^{r(0)} = \frac{\alpha\cos m\alpha(2n+1)^2}{\pi^2-4m^2\alpha^2}\frac{(n-m)!}{(n+m)!}\cdot\frac{\sin\theta_0[P_n^m(\cos\theta_0)]'}{n(n+1)k_0a^2(1+\delta_m)}\cdot\frac{[ah_n^{(2)}(k_0a)]'}{\{(n+1)[h_{n-1}^{(2)}(k_0a)]^2+n[h_{n+1}^{(2)}(k_0a)]^2\}} \tag{8}$$

where

$$[P_n^m(\cos\theta_0)]' \equiv \left\{\frac{d}{d\theta}[P_n^m(\cos\theta)]\right\}_{\theta=\theta_0}$$

$$[ah_n^{(2)}(k_0a)]' \equiv \left\{\frac{d}{dr}[rh_n^{(2)}(k_0r)]\right\}_{r=a}$$

$$\delta_m = 1 \text{ if } m = 0 \quad \text{and} \quad \delta_m = 0 \text{ if } |m| > 0.$$

Details of the derivations of (7) and (8) are available elsewhere [12]. Once $A_{mn}^{r(0)}$ and $B_{mn}^{r(0)}$ are obtained, the near-zone field $[\vec{E}^{r(0)}, \vec{H}^{r(0)}]$ of the slot is completely determined.

*B. Translation of the Near-Zone Field of the Slot from the Unprimed Coordinate System to the Primed Coordinate System*

To analyze the interaction of the near-zone field of the slot with the dielectric sphere which is described by the primed coordinate system, it was necessary to translate the near-zone field $[\vec{E}^{r(0)}, \vec{H}^{r(0)}]$ of the slot into the primed coordinates to give the first-order incident field $[\vec{E}^{i(1)}, \vec{H}^{i(1)}]$ on the dielectric sphere. Also, $[\vec{E}^{i(1)}, \vec{H}^{i(1)}]$ should be expressed in terms of vector spherical harmonics that are finite at the origin 0′. This lead to the following relation:

$$\begin{aligned}\vec{E}^{r(0)}(r,\theta,\phi) &= \vec{E}^{i(1)}(r',\theta',\phi') \\ &= \sum_{v=0}^{\infty}\sum_{u=-v}^{v}\left[A_{uv}^{i(1)}\vec{M}_{uv}^{\prime j}(r',\theta',\phi') \right. \\ &\quad \left. + B_{uv}^{i(1)}\vec{N}_{uv}^{\prime j}(r',\theta',\phi')\right] \end{aligned} \tag{9}$$

where the superscript $j$ for $\vec{M}_{uv}^{\prime j}$ and $\vec{N}_{uv}^{\prime j}$ meant that the first kind of spherical Bessel function $j_v(k_0r')$ was used for $z_n(k_0r')$, and the prime in the superscript implies that the vector spherical harmonics were expressed in terms of primed coordinates.

To equate $\vec{E}^{r(0)}(r,\theta,\phi)$ given in (2) to $\vec{E}^{i(1)}(r',\theta',\phi')$ given in (9), the vector spherical harmonics of two different coordinate systems need to be related. According to the addition theorem for vector spherical harmonics [13]–[15], $\vec{M}_{mn}^h(r,\theta,\phi)$ and $\vec{N}_{mn}^h(r,\theta,\phi)$ in unprimed coordinates can be expressed as the double summation, over the indices of $u$ and $v$, of $\vec{M}_{uv}^{\prime j}(r',\theta',\phi')$ and $\vec{N}_{uv}^{\prime j}(r',\theta',\phi')$. For our chosen geometry, since the polar axes of the two coordinate systems coincide, the index $m$ of $\vec{M}_{mn}^h(r,\theta,\phi)$ and $\vec{N}_{mn}^h(r,\theta,\phi)$ is identical to the index $u$ of $\vec{M}_{uv}^{\prime j}(r',\theta',\phi')$ and $\vec{N}_{uv}^{\prime j}(r',\theta',\phi')$ because they represent the same azimuth variation rate. With this simplification we could write

$$\begin{aligned}\vec{M}_{mn}^h(r,\theta,\phi) = \sum_{v=|m|}^{\infty}&\left[C(m,n/m,v)\vec{M}_{mv}^{\prime j}(r',\theta',\phi') \right. \\ &\left. + D(m,n/m,v)\vec{N}_{mv}^{\prime j}(r',\theta',\phi')\right] \end{aligned} \tag{10}$$

$$\begin{aligned}\vec{N}_{mn}^h(r,\theta,\phi) = \sum_{v=|m|}^{\infty}&\left[D(m,n/m,v)\vec{M}_{mv}^{\prime j}(r',\theta',\phi') \right. \\ &\left. + C(m,n/m,v)\vec{N}_{mv}^{\prime j}(r',\theta',\phi')\right] \end{aligned} \tag{11}$$

where

$$C(m,n/m,v) = (-1)^m j^{v-n} \cdot \sum_{\rho_{\min}}^{\rho_{\max}} h_\rho^{(2)}(k_0r_0)\alpha(m/\rho,n,v) \tag{12}$$

$$D(m,n/m,v) = (-1)^m j^{v-n} \cdot \sum_{\rho_{\min}}^{\rho_{\max}} h_\rho^{(2)}(k_0r_0)\beta(m/\rho,n,v) \tag{13}$$

$$\rho_{\min} = \begin{cases} |v-n|-1, & \text{for } v \neq n \\ 0, & \text{for } v = n \end{cases}; \quad \rho_{\max} = \eta + v + 1$$

$$\begin{aligned}\alpha(m/\rho,n,v) = j^\rho\Big\{&(2v+1)a(m,-m/\rho,n,v) \\ &+ jk_0r_0\frac{v+m+1}{v+1}a(m,-m/\rho,n,v+1) \\ &- jk_0r_0\frac{v-m}{v}a(m,-m/\rho,n,v-1)\Big\}\end{aligned} \tag{14}$$

$$\beta(m/\rho,n,v) = j^\rho\frac{jk_0r_0(2v+1)m}{v(v+1)}a(m,-m/\rho,n,v) \tag{15}$$

$$a(m,-m/\rho,n,v) = \frac{\int_0^\pi P_\rho(\cos\alpha)P_n^m(\cos\alpha)P_v^{-m}(\cos\alpha)\sin\alpha\,d\alpha}{\int_0^\pi\left[P_\rho(\cos\alpha)\right]^2\sin\alpha\,d\alpha}$$

or

$$\begin{aligned}a(m,-m/\rho,n,v) &= \frac{(2\rho+1)(\rho)!(v+n-\rho-1)!!}{(n+v-\rho)!!(v+\rho-n)!!(\rho+n+v+1)!!} \\ &\quad\times\sum_{\iota=0}^{\rho}(-1)^{(n-v+\rho)/2+m+\iota} \\ &\quad\cdot\frac{(n+m+\iota)!(v+\rho-m-\iota)!}{(\iota)!(\rho-\iota)!(n-m-\iota)!(v-\rho+m+\iota)!}\end{aligned} \tag{16}$$

$(t)!! = t(t-2)(t-4)\cdots 2 \text{ or } 1, \quad \text{and} \quad (0)!! = (-1)!! = 1.$

Details of the relations of (10) to (16) are available elsewhere [12].

Now, the substitution of (10) and (11) in (2) leads to

$$\begin{aligned}\vec{E}^{r(0)}(r,\theta,\phi) = \sum_{n=0}^{\infty}\sum_{m=-n}^{n}\Bigg\{&A_{mn}^{r(0)}\sum_{v=|m|}^{\infty} \\ &\cdot\left[C(m,n/m,v)\vec{M}_{mv}^{\prime j}\right. \\ &\left.+ D(m,n/m,v)\vec{N}_{mv}^{\prime j}\right] \\ &+ B_{mn}^{r(0)}\sum_{v=|m|}^{\infty}\left[D(m,n/m,v)\right.\end{aligned}$$

$$\cdot \vec{M}_{mv}^{rj} + C(m,n/m,v)\vec{N}_{mv}^{rj}\Big]\Big\}$$

$$= \sum_{v=0}^{\infty}\sum_{m=-v}^{v}\Big\{\sum_{n=|m|}^{\infty}\big[C(m,n/m,v)A_{mn}^{r(0)} + D(m,n/m,v)B_{mn}^{r(0)}\big]\vec{M}_{mv}^{rj}(r',\theta',\phi') + \sum_{n=|m|}^{\infty}\big[D(m,n/m,v)A_{mv}^{r(0)} + C(m,n/m,v)B_{mn}^{r(0)}\big]\vec{N}_{mv}^{rj}(r',\theta',\phi')\Big\}. \quad (17)$$

Since $u = m$, (9) can be rewritten as

$$\vec{E}^{ri(1)}(r',\theta',\phi') = \sum_{v=0}^{\infty}\sum_{m=-v}^{v}\big[A_{mv}^{ri(1)}\vec{M}_{mv}^{rj}(r',\theta',\phi') + B_{mv}^{ri(1)}\vec{N}_{mv}^{rj}(r',\theta',\phi')\big] \quad (18)$$

and then

$$\vec{H}^{ri(1)}(r',\theta',\phi') = \frac{j}{\eta_0}\sum_{v=0}^{\infty}\sum_{m=-v}^{v}\big[B_{mv}^{ri(1)}\vec{M}_{mv}^{rj}(r',\theta',\phi') + A_{mv}^{ri(1)}\vec{N}_{mv}^{rj}(r',\theta',\phi')\big]. \quad (19)$$

Comparing (17) with (18), we have

$$A_{mv}^{ri(1)} = \sum_{n=|m|}^{\infty}\big[C(m,n/m,v)A_{mn}^{r(0)} + D(m,n/m,v)B_{mn}^{r(0)}\big] \quad (20)$$

$$B_{mv}^{ri(1)} = \sum_{n=|m|}^{\infty}\big[D(m,n/m,v)A_{mn}^{r(0)} + C(m,n/m,v)B_{mn}^{r(0)}\big] \quad (21)$$

or in a matrix form as

$$\begin{bmatrix} A_{mv}^{ri(1)} \\ B_{mv}^{ri(1)} \end{bmatrix} = \sum_{n=|m|}^{\infty}\begin{bmatrix} C(m,n/m,v), & D(m,n/m,v) \\ D(m,n/m,v), & C(m,n/m,v) \end{bmatrix} \cdot \begin{bmatrix} A_{mn}^{r(0)} \\ B_{mn}^{r(0)} \end{bmatrix}. \quad (22)$$

Since $A_{mn}^{r(0)}$ and $B_{mn}^{r(0)}$ have been determined in Section III-B, $A_{mv}^{ri(1)}$ and $B_{mn}^{ri(1)}$ can be calculated from (22). Then the first-order incident field $[\vec{E}^{ri(1)}, \vec{H}^{ri(1)}]$ to the dielectric sphere is completely determined.

### C. Transmitted Field in and Scattered Field by the Dielectric Sphere

The first-order incident field $[\vec{E}^{ri(1)}, \vec{H}^{ri(1)}]$ on the dielectric sphere generates the first-order transmitted field $[\vec{E}^{rt(1)}, \vec{H}^{rt(1)}]$ in the dielectric sphere and the first-order scattered field $[\vec{E}^{rs(1)}, \vec{H}^{rs(1)}]$ by the dielectric sphere. The latter two fields can be expressed in terms of vector spherical harmonics as follows:

$$\vec{E}^{rt(1)}(r',\theta',\phi') = \sum_{v=0}^{\infty}\sum_{m=-v}^{v}\big[A_{mv}^{rt(1)}\vec{M}_{mv}^{rj}(r',\theta',\phi') + B_{mv}^{rt(1)}\vec{N}_{mv}^{rj}(r',\theta',\phi')\big] \quad (23)$$

$$\vec{H}^{rt(1)}(r',\theta',\phi') = \frac{j}{\eta_d}\sum_{v=0}^{\infty}\sum_{m=-v}^{v}\big[B_{mv}^{rt(1)}\vec{M}_{mv}^{rj}(r',\theta',\phi') + A_{mv}^{rt(1)}\vec{N}_{mv}^{rj}(r',\theta',\phi')\big] \quad (24)$$

where

$$\eta_d = \sqrt{\mu_0/\epsilon(1 - j\sigma/\omega\epsilon)}$$

and

$$\vec{E}^{rs(1)}(r',\theta',\phi') = \sum_{v=0}^{\infty}\sum_{m=-v}^{v}\big[A_{mv}^{rs(1)}\vec{M}_{mv}^{rh}(r',\theta',\phi') + B_{mv}^{rs(1)}\vec{N}_{mv}^{rh}(r',\theta',\phi')\big] \quad (25)$$

$$\vec{H}^{rs(1)}(r',\theta',\phi') = \frac{j}{\eta_0}\sum_{v=0}^{\infty}\sum_{m=-v}^{v}\big[B_{mv}^{rs(1)}\vec{M}_{mv}^{rh}(r',\theta',\phi') + A_{mv}^{rs(1)}\vec{N}_{mv}^{rh}(r',\theta',\phi')\big]. \quad (26)$$

It is noted that the propagation constant for $\vec{M}_{mv}^{rj}$ and $\vec{N}_{mv}^{rj}$ in (23) and (24) is $k_d$ and that for $\vec{M}_{mv}^{rh}$ and $\vec{N}_{mv}^{rh}$ in (25) and (26) is $k_0$. The unknown coefficients $A_{mv}^{rt(1)}$, $B_{mv}^{rt(1)}$, $A_{mv}^{rs(1)}$, and $B_{mv}^{rs(1)}$ are determined based on the boundary conditions on the surface of the dielectric sphere at $r' = b$:

$$E_\theta^{rt(1)}(b,\theta',\phi') = E_\theta^{ri(1)}(b,\theta',\phi') + E_\theta^{rs(1)}(b,\theta',\phi') \quad (27)$$

$$H_\theta^{rt(1)}(b,\theta',\phi') = H_\theta^{ri(1)}(b,\theta',\phi') + H_\theta^{rs(1)}(b,\theta',\phi'). \quad (28)$$

The substitution of (18), (23), and (25) in (27), and (19), (24), and (26) in (28) yields the following equations:

$$A_{mv}^{rt(1)} j_v(k_d b) = A_{mv}^{ri(1)} j_v(k_0 b) + A_{mv}^{rs(1)} h_v^{(2)}(k_0 b) \quad (29)$$

$$B_{mv}^{rt(1)}[bj_v(k_d b)]'/k_d b = \big\{B_{mv}^{ri(1)}[bj_v(k_0 b)]' + B_{mv}^{rs(1)}[bh_v^{(2)}(k_0 b)]'\big\}/k_0 b \quad (30)$$

$$B_{mv}^{rt(1)} j_v(k_d b) = \frac{\eta_d}{\eta_0}\big[B_{mv}^{ri(1)} j_v(k_0 b) + B_{mv}^{rs(1)} h_v^{(2)}(k_0 b)\big] \quad (31)$$

$$A_{mv}^{rt(1)}[bj_v(k_d b)]'/k_d b = \frac{\eta_d}{\eta_0}\frac{1}{k_0 b}\big\{A_{mv}^{ri(1)}[bj_v(k_0 b)]' + A_{mv}^{rs(1)}[bh_v^{(2)}(k_0 b)]'\big\}. \quad (32)$$

From (29) to (32), the transmission coefficients $A_{mv}^{rt(1)}$ and $B_{mv}^{rt(1)}$, and the scattering coefficients $A_{mv}^{rs(1)}$ and $B_{mv}^{rs(1)}$ of the

dielectric sphere, can be determined in terms of the incident coefficients $A_{mv}^{i(1)}$ and $B_{mv}^{i(1)}$ as

$$\begin{bmatrix} A_{mv}^{t(1)} \\ B_{mv}^{t(1)} \end{bmatrix} = \begin{bmatrix} T_v^{(A)} & 0 \\ 0 & T_v^{(B)} \end{bmatrix} \begin{bmatrix} A_{mv}^{i(1)} \\ B_{mv}^{i(1)} \end{bmatrix} \tag{33}$$

and

$$\begin{bmatrix} A_{mv}^{s(1)} \\ B_{mv}^{s(1)} \end{bmatrix} = \begin{bmatrix} S_v^{(A)} & 0 \\ 0 & S_v^{(B)} \end{bmatrix} \begin{bmatrix} A_{mv}^{t(1)} \\ B_{mv}^{t(1)} \end{bmatrix} \tag{34}$$

where

$$T_v^{(A)} = \frac{\eta_d k_d j_v(k_0 b)[b h_v^{(2)}(k_0 b)]' - \eta_d k_d h_v^{(2)}(k_0 b)[b j_v(k_0 b)]'}{\eta_d k_d j_v(k_d b)[b h_v^{(2)}(k_0 b)]' - \eta_0 k_0 h_v^{(2)}(k_0 b)[b j_v(k_d b)]'} \tag{35}$$

$$T_v^{(B)} = \frac{\eta_d k_d j_v(k_0 b)[b h_v^{(2)}(k_0 b)]' - \eta_d k_d h_v^{(2)}(k_0 b)[b j_v(k_0 b)]'}{\eta_0 k_d j_v(k_d b)[b h_v^{(2)}(k_0 b)]' - \eta_d k_0 h_v^{(2)}(k_0 b)[b j_v(k_d b)]'} \tag{36}$$

$$S_v^{(A)} = \frac{T_v^{(A)} j_v(k_d b) - j_v(k_0 b)}{h_v^{(2)}(k_0 b)} \tag{37}$$

$$S_v^{(B)} = \frac{T_v^{(B)} \eta_0 j_v(k_d b) - \eta_d j_v(k_0 b)}{h_v^{(2)}(k_0 b)}. \tag{38}$$

The first-order transmitted field $[\vec{E}^{t(1)}, \vec{H}^{t(1)}]$ in the dielectric sphere dissipates inside the dielectric sphere, while a portion of the first-order scattered field $[\vec{E}^{s(1)}, \vec{H}^{s(1)}]$ by the dielectric sphere becomes the first-order incident field $[\vec{E}^{i(1)}, \vec{H}^{i(1)}]$ to the conducting sphere.

### *D. Translation of the Scattered Field by the Dielectric Sphere from the Primed Coordinate Systems to the Unprimed Coordinate System*

The first-order scattered field $[\vec{E}^{s(1)}, \vec{H}^{s(1)}]$ by the dielectric sphere can be translated from the primed coordinate system to the unprimed coordinate system to give the first-order incident field $[\vec{E}^{i(1)}, \vec{H}^{i(1)}]$ on the conducting sphere. This incident field is scattered by the conducting sphere and a portion of it becomes the second-order incident field to the dielectric sphere.

The appropriate expressions for $[\vec{E}^{i(1)}, \vec{H}^{i(1)}]$ are

$$\vec{E}^{i(1)}(r,\theta,\phi) = \sum_{n=0}^{\infty} \sum_{m=-n}^{n} \left[ A_{mn}^{i(1)} \vec{M}_{mn}^{j}(r,\theta,\phi) + B_{mn}^{i(1)} \vec{N}_{mn}^{j}(r,\theta,\phi) \right] \tag{39}$$

$$\vec{H}^{i(1)}(r,\theta,\phi) = \frac{j}{\eta_0} \sum_{n=0}^{\infty} \sum_{m=-n}^{n} \left[ B_{mn}^{i(1)} \vec{M}_{mn}^{j}(r,\theta,\phi) + A_{mn}^{i(1)} \vec{N}_{mn}^{j}(r,\theta,\phi) \right]. \tag{40}$$

To equate $[\vec{E}^{i(1)}, \vec{H}^{i(1)}]$ of (39) and (40) to $[\vec{E}^{s(1)}, \vec{H}^{s(1)}]$ of (25) and (26), we need the following addition theorem [13]–[15]:

$$\vec{M}_{mv}^{rh}(r',\theta',\phi') = \sum_{n=|m|}^{\infty} \left[ C'(m,v/m,n) \vec{M}_{mn}^{j}(r,\theta,\phi) + D'(m,v/m,n) \vec{N}_{mn}^{j}(r,\theta,\phi) \right] \tag{41}$$

$$\vec{N}_{mv}^{rh}(r',\theta',\phi') = \sum_{n=|m|}^{\infty} \left[ D'(m,v/m,n) \vec{M}_{mn}^{j}(r,\theta,\phi) + C'(m,v/m,n) \vec{N}_{mn}^{j}(r,\theta,\phi) \right] \tag{42}$$

where

$$C'(m,v/m,n) = (-1)^m j^{n-v} \sum_{\rho_{\min}}^{\rho_{\max}} h_\rho^{(2)}(k_0 r_0) \alpha^*(m/\rho, v, n) \tag{43}$$

$$D'(m,v/m,n) = (-1)^m j^{n-v} \sum_{\rho_{\min}}^{\rho_{\max}} h_\rho^{(2)}(k_0 r_0) \beta^*(m/\rho, v, n) \tag{44}$$

and $\alpha^*(m/\rho, v, n)$ and $\beta^*(m/\rho, v, n)$ are the conjugates of $\alpha(m/\rho, v, n)$ and $\beta(m/\rho, v, n)$ which have been defined in (14) and (15).

The substitution of (41) and (42) in (25) leads to

$$\vec{E}^{rs(1)}(r',\theta',\phi') = \sum_{n=0}^{\infty} \sum_{m=-n}^{n} \left\{ \sum_{v=|m|}^{\infty} \left[ A_{mv}^{rs(1)} C'(m,v/m,n) + B_{mv}^{rs(1)} D'(m,v/m,n) \right] \cdot \vec{M}_{mn}^{j}(r,\theta,\phi) + \sum_{v=|m|}^{\infty} \left[ A_{mv}^{rs(1)} D'(m,v/m,n) + B_{mv}^{rs(1)} D'(m,v/m,n) \right] \vec{N}_{mn}^{j}(r,\theta,\phi) \right\}. \tag{45}$$

By setting $\vec{E}^{i(1)}$ of (39) equal to $\vec{E}^{rs(1)}$ of (45), we have

$$\begin{bmatrix} A_{mn}^{i(1)} \\ B_{mn}^{i(1)} \end{bmatrix} = \sum_{v=|m|}^{\infty} \begin{bmatrix} C'(m,v/m,n), & D'(m,v/m,n) \\ D'(m,v/m,n), & C'(m,v/m,n) \end{bmatrix} \cdot \begin{bmatrix} A_{mv}^{rs(1)} \\ B_{mv}^{rs(1)} \end{bmatrix}. \tag{46}$$

With $A_{mv}^{rs(1)}$ and $B_{mv}^{rs(1)}$ already determined in Section III-C, $A_{mn}^{i(1)}$ and $B_{mn}^{i(1)}$ can be calculated from (46). Thus, the first-order incident field $[\vec{E}^{i(1)}, \vec{H}^{i(1)}]$ to the conducting sphere is completely determined.

### *E. Scattered Field by the Conducting Sphere*

The first-order incident field $[\vec{E}^{i(1)}, \vec{H}^{i(1)}]$ on the conducting sphere is completely scattered at the surface of the conducting sphere. The radiating slot on the conducting

sphere is narrow so that it is reasonable to assume the conducting sphere to have a closed surface in analyzing the scattered field by the conducting sphere.

The first-order scattered field $[E^{s(1)}, H^{s(1)}]$ by the conducting sphere can be expressed as

$$\vec{E}^{s(1)}(r,\theta,\phi) = \sum_{n=0}^{\infty}\sum_{m=-n}^{n}\left[A_{mn}^{s(1)}\vec{M}_{mn}^{h}(r,\theta,\phi) + B_{mn}^{s(1)}\vec{N}_{mn}^{h}(r,\theta,\phi)\right] \quad (47)$$

$$\vec{H}^{s(1)}(r,\theta,\phi) = \frac{j}{\eta_0}\sum_{n=0}^{\infty}\sum_{m=-n}^{n}\left[B_{mn}^{s(1)}\vec{M}_{mn}^{h}(r,\theta,\phi) + A_{mn}^{s(1)}\vec{N}_{mn}^{h}(r,\theta,\phi)\right]. \quad (48)$$

It is noted that the propagation constant $k$ for $\vec{M}_{mn}^{h}$ and $\vec{N}_{mn}^{h}$ in (47) and (48) is $k_0$. The coefficients $A_{mn}^{s(1)}$ and $B_{mn}^{s(1)}$ can be determined from the boundary condition on the surface of the conducting sphere at $r = a$

$$E_{\theta}^{s(1)}(a,\theta,\phi) + E_{\theta}^{i(1)}(a,\theta,\phi) = 0. \quad (49)$$

Equation (49) leads to

$$A_{mn}^{s(1)}h_n^{(2)}(k_0a) = -A_{mn}^{i(1)}j_n(k_0a) \quad (50)$$

$$B_{mn}^{s(1)}\left[ah_n^{(2)}(k_0a)\right]' = -B_{mn}^{i(1)}\left[aj_n(k_0a)\right]' \quad (51)$$

or, in a matrix form, as

$$\begin{bmatrix} A_{mn}^{s(1)} \\ B_{mn}^{s(1)} \end{bmatrix} = \begin{bmatrix} S_n^{(A)} & 0 \\ 0 & S_n^{(B)} \end{bmatrix}\begin{bmatrix} A_{mn}^{i(1)} \\ B_{mn}^{i(1)} \end{bmatrix} \quad (52)$$

with

$$S_n^{(A)} = -j_n(k_0a)/h_n^{(2)}(k_0a) \quad (53)$$

$$S_n^{(B)} = -\left[aj_n(k_0a)\right]'/\left[ah_n^{(2)}(k_0a)\right]'. \quad (54)$$

Up to this point, the first-order scattered field $[\vec{E}^{s(1)}, \vec{H}^{s(1)}]$ by the conducting sphere is completely determined. This field can be translated into the primed coordinate system to give the second-order incident field $[\vec{E}'^{i(2)}, \vec{H}'^{i(2)}]$ to the dielectric sphere. After that, the second-order fields can be determined by repeating the process of Sections III-B to III-E.

### *F. Multiple Transmitted and Scattered Fields by Iterative Calculation*

In the preceding sections, the first-order fields have been determined. The second-order incident field to the dielectric sphere will initiate the second-round calculation of the second-order transmitted and scattered fields. After that, the calculation of the third-order fields can be repeated. This iterative calculation of higher-order fields will be continued until the sums of multiple partial transmitted fields and multiple partial scattered fields converge.

The calculation of the $l$th-order fields starts from the $(l-1)$th-order scattered field by the conducting sphere as follows:

$$\begin{bmatrix} A_{mv}'^{i(l)} \\ B_{mv}'^{i(l)} \end{bmatrix} = \sum_{n=|m|}^{\infty}\begin{bmatrix} C(m,n/m,v) & D(m,n/m,v) \\ D(m,n/m,v) & C(m,n/m,v) \end{bmatrix} \cdot \begin{bmatrix} A_{mn}^{s(l-1)} \\ B_{mn}^{s(l-1)} \end{bmatrix} \quad (55)$$

$$\begin{bmatrix} A_{mv}'^{t(l)} \\ B_{mv}'^{t(l)} \end{bmatrix} = \begin{bmatrix} T_v'^{(A)} & 0 \\ 0 & T_v'^{(B)} \end{bmatrix}\begin{bmatrix} A_{mv}'^{i(l)} \\ B_{mv}'^{i(l)} \end{bmatrix} \quad (56)$$

$$\begin{bmatrix} A_{mv}'^{s(l)} \\ B_{mv}'^{s(l)} \end{bmatrix} = \begin{bmatrix} S_v'^{(A)} & 0 \\ 0 & S_v'^{(B)} \end{bmatrix}\begin{bmatrix} A_{mv}'^{i(l)} \\ B_{mv}'^{i(l)} \end{bmatrix} \quad (57)$$

$$\begin{bmatrix} A_{mn}^{i(l)} \\ B_{mn}^{i(l)} \end{bmatrix} = \sum_{v=|m|}^{\infty}\begin{bmatrix} C'(m,v/m,n) & D'(m,v/m,n) \\ D'(m,v/m,n) & C'(m,v/m,n) \end{bmatrix} \cdot \begin{bmatrix} A_{mv}'^{s(l)} \\ B_{mv}'^{s(l)} \end{bmatrix} \quad (58)$$

and

$$\begin{bmatrix} A_{mn}^{s(l)} \\ B_{mn}^{s(l)} \end{bmatrix} = \begin{bmatrix} S_n^{(A)} & 0 \\ 0 & S_n^{(B)} \end{bmatrix}\begin{bmatrix} A_{mn}^{i(l)} \\ B_{mn}^{i(l)} \end{bmatrix}. \quad (59)$$

After the determination of $A_{mn}^{s(l)}$ and $B_{mn}^{s(l)}$, the $(l+1)$th-order fields can be calculated by repeating the process of (55) to (59). The total transmitted field in the dielectric sphere is

$$\vec{E}'^{t}(r',\theta',\phi') = \sum_{l=1}^{L}\sum_{v=0}^{\infty}\sum_{m=-v}^{v}\left[A_{mv}'^{t(l)}M_{mv}'^{j}(r',\theta',\phi') + B_{mv}'^{t(l)}N_{mn}'^{j}(r',\theta',\phi')\right] \quad (60)$$

$$\vec{H}'^{t}(r',\theta',\phi') = \frac{j}{\eta_d}\sum_{l=1}^{L}\sum_{v=0}^{\infty}\sum_{m=-v}^{v}\left[B_{mv}'^{t(l)}\vec{M}_{mv}'^{j}(r',\theta',\phi') + A_{mv}'^{t(l)}\vec{N}_{mv}'^{j}(r',\theta',\phi')\right]. \quad (61)$$

Equations (60) and (61) imply the summations of multiple transmitted fields from the first-order up to the $L$th-order. The selection of an upper limit is dictated by the convergence of the total transmitted field given in (60) and (61). This limit is dependent on the electric dimensions of the spheres and the distance between the spheres. In our numerical example given in the following sections, the choice of $L = 10$ was found to be sufficient.

Similarly, the total scattered field surrounding the spheres is obtained as

$$[\vec{E}^{s}, \vec{H}^{s}] = [\vec{E}^{r(0)}, \vec{H}^{r(0)}] + \sum_{l=1}^{L}\cdot[\vec{E}^{s(l)}, \vec{H}^{s(l)}] + \sum_{l=1}^{L}[\vec{E}'^{s(l)}, \vec{H}'^{s(l)}]. \quad (62)$$

Of course, the two coordinate systems used in the fields of (62) need to be unified in the calculation of the total scattered field surrounding the spheres.

## IV. Numerical Calculation and Results

The main result of the analysis in the preceding sections is the total transmitted field in the dielectric sphere because it represents the total induced field in a biological body placed in the proximity of an aperture EM source. The numerical calculation of this result is discussed here.

The total transmitted electric field in the dielectric sphere given in (60) can be rewritten as

$$\begin{aligned}\vec{E}'(r',\theta',\phi') &= \sum_{v=0}^{\infty}\sum_{m=-v}^{v}\left\{\left[\sum_{l=1}^{L}A_{mv}'^{(l)}\right]\vec{M}_{mv}'^{j}(r',\theta',\phi')\right.\\ &\quad\left.+\left[\sum_{l=1}^{L}B_{mv}'^{(l)}\right]\vec{N}_{mv}'^{j}(r',\theta',\phi')\right\}\\ &= \sum_{m=-\infty}^{\infty}\sum_{v=|m|}^{\infty}\left\{A_{mv}'\vec{M}_{mv}'^{j}(r',\theta',\phi')\right.\\ &\quad\left.+B_{mv}'\vec{N}_{mv}'^{j}(r',\theta',\phi')\right\} \qquad (63)\end{aligned}$$

where the total transmission coefficients $A_{mv}'$ and $B_{mv}'$ are defined as

$$A_{mv}' = \sum_{l=1}^{L}A_{mv}'^{(l)} \qquad (64)$$

$$B_{mv}' = \sum_{l=1}^{L}B_{mv}'^{(l)}. \qquad (65)$$

Also, the order of summation over $m$ and $v$ in (63) have been reversed to facilitate the computation. Since the value of the product of the coefficient and the vector spherical harmonic decreases rapidly as the values of $m$ and $v$ increase, it is possible to limit the computation for $m=0$ to $|m|=M$ and for $v=0$ to $v=V$. Thus, (63) can be further simplified to

$$\begin{aligned}\vec{E}'(r',\theta',\phi') &= \sum_{m=0}^{M}\sum_{v=m}^{V}\left\{A_{mv}'\vec{M}_{mv}'^{j}(r',\theta',\phi')\right.\\ &\quad+B_{mv}'\vec{N}_{mv}'^{j}(r',\theta',\phi')\\ &\quad+A_{-mv}'\vec{M}_{-mv}'^{j}(r',\theta',\phi')\\ &\quad\left.+B_{-mv}'\vec{N}_{-mv}'^{j}(r',\theta',\phi')\right\}\frac{1}{1+\delta_m} \qquad (66)\end{aligned}$$

where $\delta_m=1$ for $m=0$ and $\delta_m=0$ for $m\neq 0$.

To use (66), we need the functions of negative $m$ used in the analysis as given below:

$$P_n^{-m}(\cos\theta) = (-1)^m\frac{(n-m)!}{(n+m)!}P_n^m(\cos\theta) \qquad (67)$$

$$A_{mn}^{r(0)} = (-1)^{m+1}\frac{(n-m)!}{(n+m)!}A_{-mn}^{r(0)} \qquad (68)$$

$$B_{mn}^{r(0)} = (-1)^m\frac{(n-m)!}{(n+m)!}B_{-mn}^{r(0)} \qquad (69)$$

$$C(-m,n/-m,v) = \frac{(n-m)!}{(n+m)!}\frac{(v+m)!}{(v-m)!}\cdot C(m,n/m,v) \qquad (70)$$

$$D(-m,n/-m,v) = -\frac{(n-m)!}{(n+m)!}\frac{(v+m)!}{(v-m)!}\cdot D(m,n/m,v) \qquad (71)$$

$$C'(-m,v/-m,n) = \frac{(v-m)!}{(v+m)!}\frac{(n+m)!}{(n-m)!}\cdot C'(m,v/m,n) \qquad (72)$$

$$D'(-m,v/-m,n) = -\frac{(v-m)!}{(v+m)!}\frac{(n+m)!}{(n-m)!}\cdot D'(m,n/m,v) \qquad (73)$$

$$\vec{M}_{-mv} = (-1)^m\frac{(v-m)!}{(v+m)!}\vec{M}_{mv}^{*} \qquad (74)$$

$$\vec{N}_{-mv} = (-1)^m\frac{(v-m)!}{(v+m)!}\vec{N}_{mv}^{*}. \qquad (75)$$

Derivations of the above relations are available elsewhere [12].

In the numerical calculation, we first assign a value for $m$ and then compute $A_{mv}'$ and $B_{mv}'$ for $v=|m|$ to $v=V$, and also compute $C(m,n/m,v)$, $D(m,n/m,v)$, $C'(m,v/m,n)$, and $D'(m,v/m,n)$ as two-dimensional arrays for the indices of $n$ and $v$. For the numerical example to be discussed in the following sections, it was found to be sufficient to set $M=10$ and $V=50$, and also $L=10$ as mentioned before.

### A. Geometry of Numerical Example

The geometry of the numerical example is shown in Fig. 1 with the following assumed dimensions. The radius of the conducting sphere (microwave oven) $a$ is 20 cm. The location of the radiating slot (leakage gap) is at $\theta_0=10°$, and the slot length subtends an azimuth angle of $2\alpha=60°$. The slot radiates at a frequency of 2.45 GHz with a slot field given in (1), which indicates a potential difference of 1 V across the slot at its center. The dielectric sphere (simulated body) has a radius of $b=25$ cm and a conductivity of $\sigma=2.21$ S/m and a relative permittivity of $\epsilon/\epsilon_0=47$ at 2.45 GHz. The distance $r_0$ between the centers of the two spheres is assumed to be variable. Based on this geometry, the following results have been computed.

### B. Coupling Effect Between the Dielectric Sphere and the Conducting Sphere

The most important goal in this study was to estimate the coupling effect between the source (conducting sphere) and the body (dielectric sphere). In calculating the total induced field in the body excited by the near-zone field of an aperture source on a conducting structure, if the body–source coupling effect is ignored, as in most existing studies, the total induced field in the body can be determined exclusively by the first-order transmitted field $[\vec{E}'^{(1)},\vec{H}'^{(1)}]$ in the dielectric sphere. This ignores the multiple scattering phenomenon between the two spheres. In fact, the actual total induced field inside the body should be determined by the sum of all the multiple partial transmitted fields $[\vec{E}'=\sum_{l=1}^{L}\vec{E}'^{(l)},\ \vec{H}'=\sum_{l=1}^{L}H'^{(l)}]$ as

mentioned before. Thus, by comparing the values of $\vec{E}'$ and $\vec{E}'^{(1)}$, both the body–source coupling effect and the error caused by neglecting this effect can be estimated.

To examine the difference between $\vec{E}'$ and $\vec{E}'^{(1)}$, it was only necessary to calculate the transmitted field at a representative point in the dielectric sphere. That representative point was chosen to be at $r'=b$, $\theta'=17\pi/18$, and $\phi'=0$, a point directly facing the radiating slot. The local SAR or the dissipated power density at that point was then computed as a function of $r_0$, the distance between the centers of the two spheres. The local SAR at the representative point was calculated as

$$P=1/2\sigma\left|\sum_{l=1}^{L}\vec{E}'^{(l)}\right|^2 \text{ in (mW/Kg) or (W/m}^3\text{)}$$

and the corresponding value by ignoring the body–source coupling was calculated as

$$P_1=1/2\sigma|\vec{E}'^{(1)}|^2 \text{ in (mW/Kg) or (W/m}^3\text{)}.$$

The percentage error caused by the neglecting of the body–source coupling was indicated by

$$\text{Error}=|P-P_1|/P \text{ in (\%)}.$$

Numerical values of $P$, $P_1$, and Error as functions of $r_0$ are shown in Table I and the values of $P$ and $P_1$ are graphically compared in Fig. 3. It is seen in Table I that, when $r_0=48$ cm (minimum distance between the two sphere = 3 cm), $P=0.287$ mW/Kg, $P_1=0.448$ mW/Kg, and neglecting of the body–source coupling causes an over-estimation of SAR by 56.4 percent; on the other hand, it may cause an underestimation of SAR by 11.85 percent when $r_0=50$ cm. The behaviors of $P$ and $P_1$ as functions of $r_0$ can be easily observed in Fig. 3. The value of $P_1$ decreases smoothly with the increase of $r_0$, while the value of $P$ fluctuates in both sides of the $P_1$ curve. The values of $P_1$ and $P$ converge when $r_0$ becomes large as expected because, for large $r_0$, the higher order fields become insignificant and the multiple scattering phenomenon may be ignored. The conclusion that can be drawn from the results of Table I and Fig. 3 is the following: In the analysis of the interaction between a body and the near-zone field of an aperture source on a conducting structure, neglecting the body–source coupling will cause a serious error.

TABLE I
THE LOCAL SAR AT A REPRESENTATIVE POINT ($r'=b$, $\theta'=17\pi/18$, AND $\phi'=0$) ON THE SURFACE OF THE DIELECTRIC SPHERE AS A FUNCTION OF THE SEPARATION BETWEEN THE SPHERES, COMPUTED FOR THE CASES OF WITH ($P$) AND WITHOUT ($P_1$) TAKING INTO ACCOUNT THE BODY–SOURCE COUPLING EFFECT. THE PERCENTAGE ERROR CAUSED BY THE NEGLIGENCE OF THE BODY–SOURCE COUPLING EFFECT IS ALSO INCLUDED.

| $r_0$ (cm) | local SAR with body-source coupling $P=\frac{1}{2}\sigma[\sum_{l=1}^{L}\vec{E}^{t(l)}]^2$ | local SAR without body-source coupling $P_1=\frac{1}{2}\sigma[\vec{E}^{t(1)}]^2$ | percentage error $\lvert P-P_1\rvert/P$ |
|---|---|---|---|
| 48 | 0.2866 (mW/Kg) | 0.4483 (mW/Kg) | 56.41 % |
| 50 | 0.2800 | 0.2468 | 11.85 |
| 52 | 0.1718 | 0.1505 | 12.42 |
| 54 | 0.0780 | 0.0955 | 22.46 |
| 56 | 0.0679 | 0.0623 | 8.17 |
| 58 | 0.0449 | 0.0417 | 7.89 |
| 60 | 0.0246 | 0.0283 | 15.13 |
| 70 | 0.0060 | 0.0056 | 6.0 |
| 80 | 0.0018 | 0.0018 | 1.3 |

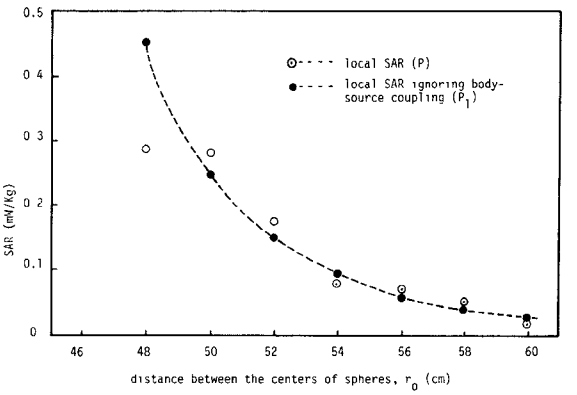


Fig. 3. The local SAR at a representative point ($r'=b$, $\theta'=17\pi/18$, and $\phi'=0$) on the surface of the dielectric sphere as a function of the separation between the spheres, computed for the cases of with and without taking into account of the body–source coupling effect.

### C. Penetration of Transmitted Field in the Dielectric Sphere

To study the nature of the transmitted field as it penetrates into the dielectric sphere, the transmitted field was calculated as a function of the radial coordinate $r'$ starting from the representative point, $r'=b$, $\theta'=17\pi/18$, and $\phi'=0$, toward the center of the dielectric sphere. For this calculation, the distance $r_0$ between the centers of the two spheres was assumed to be 50 cm. The distribution of the SAR as a function of $r'$ is indicated in Table II and shown graphically in Fig. 4. The SAR has a maximum value at the surface of the dielectric sphere ($r'=b$) and decays exponentially toward the center of the sphere. The penetration depth, the distance for the SAR to decay to $(1/e)^2$ times the maximum value at the surface, is determined from Fig. 4 to be about 1.75 cm. This value is very close to the penetration depth of 1.7 cm for the plane geometry at 2.54 GHz.

### D. Distribution of the SAR on the Surface of the Dielectric Sphere

The induced EM field or the induced SAR in the dielectric sphere has its maximum value at the surface of the sphere and then decays exponentially toward the center of the sphere. Thus, distribution of the SAR inside the sphere can best be described by the distribution of the SAR on the surface of tthe sphere. It was found unexpectedly that the distribution of the SAR on the surface of the dielectric sphere varies greatly as a function of the distance between the two spheres. This phenomenon is due to the complexity

TABLE II
THE DISTRIBUTION OF THE SAR ALONG A RADIUS STARTING FROM A SURFACE POINT ($r' = b$, $\theta' = 17\pi/18$, AND $\phi' = 0$) TOWARD THE CENTER OF THE DIELECTRIC SPHERE. THE DISTANCE BETWEEN THE CENTERS OF THE SPHERES ($r_0$) IS 50 cm FOR THIS CASE.

| x (mm) | 0 | 5 | 10 | 15 | 20 |
|---|---|---|---|---|---|
| P(mW/Kg) | 0.2800 | 0.1580 | 0.0892 | 0.0504 | 0.0284 |
| x (mm) | 25 | 30 | 35 | 40 | 45 |
| P(mW/Kg) | 0.0161 | 0.0091 | 0.0051 | 0.0029 | 0.0016 |

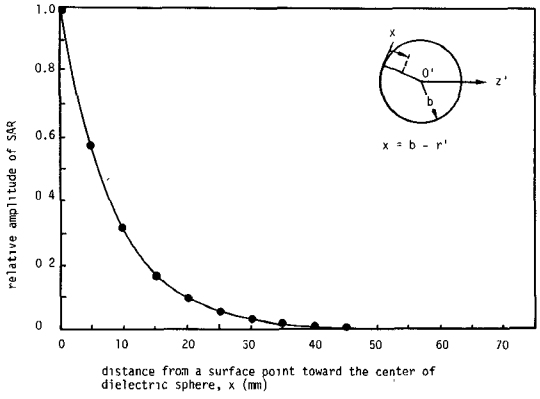


Fig. 4. The distribution of the SAR along a radius starting from a surface point ($r' = b$, $\theta' = 17\pi/18$, and $\phi' = 0$) toward the center of the dielectric sphere.

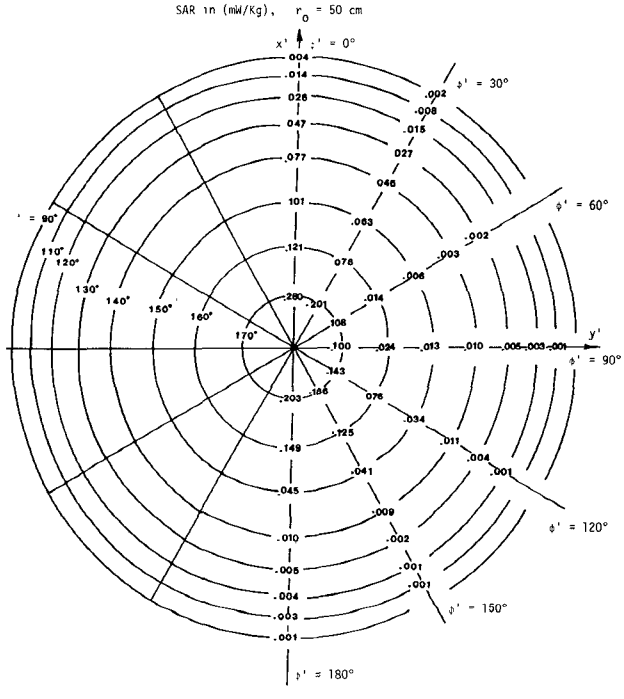


Fig. 5. The distribution of SAR's on the surface of the dielectric sphere that faces the radiating slot on the conducting sphere. The distance between the centers of the spheres is 50 cm.

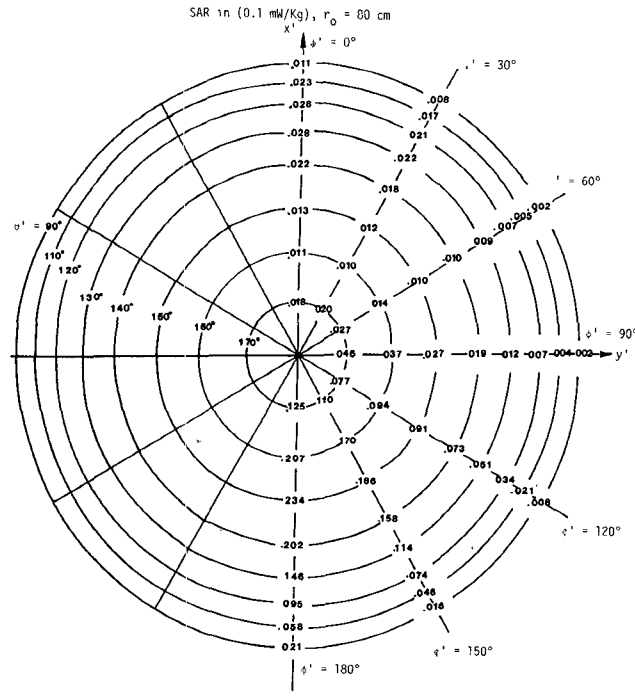


Fig. 6. The distribution of SAR's on the surface of the dielectric sphere that faces the radiating slot on the conducting sphere. The distance between the centers of the spheres is 80 cm. The unit of SAR is 0.1 mW/Kg for this case.

of the near-zone field of the slot and also by the multiple scattering of the EM wave between the two spheres.

Fig. 5 shows the distribution of the SAR on the surface of the dielectric sphere looking from the $\theta' = 180°$ axis, or it is the distribution of the SAR on that side of the surface of the dielectric sphere which faces the radiating slot on the conducting sphere. The distance between the centers of the two spheres is 50 cm for this case, and the calculated values of SAR's are given in mW/Kg. It is observed in Fig. 5 that the maximum SAR occurs near $\theta' = 175°$ and $\phi' = 0°$, the region directly facing the radiating slot. The value of SAR then decays when moving away from this maximum SAR region toward the smaller $\theta$'s. Eventually, the SAR is reduced to an insignificant value in the shadow region of $\theta' < 90°$.

Fig. 6 shows a similar distribution of the SAR on the surface of the dielectric sphere when the distance between the centers of the two spheres is increased to 80 cm. The values of SAR's are given in 0.1 mW/Kg. The distribution of the SAR shown in Fig. 6 indicates that the region of the maximum SAR is shifted to the lower half of the sphere from the upper half, the region directly facing the slot. This unexpected phenomenon can be explained by examining the radiation pattern of the far-zone field maintained by the slot on the conducting sphere. At a distance of 80 cm from the center of the conducting sphere, the slot maintains practically a far-zone field and its $E$-plane radiation pattern is shown in Fig. 7. This radiation pattern contains many lobes, and it clearly indicates that the slot maintains a stronger field at the lower half of the dielectric sphere than at the upper half. This phenomenon, combined with

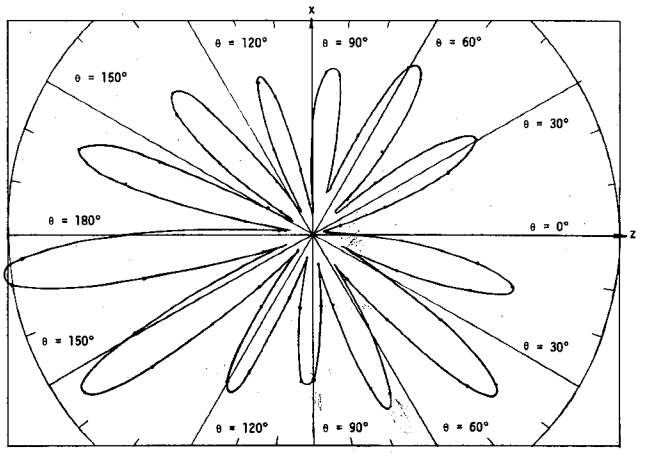


Fig. 7. *E*-plane radiation pattern maintained by a radiating slot on a conducting sphere of 20-cm radius at 2.45 GHz. Slot location: $\phi = 10°$, $-30° \leqslant \phi \leqslant 30°$, and $r = 20$ cm.

the fact that the multiple scattering effect is insignificant when the spheres are separated by 80 cm, should explain why a higher SAR is induced in the lower half of the dielectric sphere.

It is worth noting that the slot, in fact, radiates more power in the back side of the conducting sphere, as can be observed in Fig. 7. This unusual phenomenon is caused by the surface current excited by the slot on the surface of the conducting sphere which is electrically large in dimension at 2.45 GHz. This same phenomenon has been reported in a previous study [16].

The results given in this section indicate that the distribution of the SAR inside the body induced by the near-zone field of an aperture source on a conducting structure is strongly dependent on the distance between the body and the source, and neglecting the body–source coupling may yield an erroneous SAR distribution in the body.

## V. Concluding Remark

This study presents an exact solution to an idealized problem of the interaction between the near-zone field of an aperture source on a conducting structure and a human body in proximity. The analysis is very complex, and the results require an extensive numerical computation. This type of analysis is not recommended for usual practical situations that may involve quite different geometries. However, the main purpose of this study was to evaluate the effect of the body–source coupling, and this could be achieved only through an exact solution. Findings of this study lead to the warning that, if the body–source coupling effect is ignored in the study of the interaction between the near-zone field of an aperture source on a conducting structure and a human body, a serious error in the estimate of induced SAR in the body may result. On the other hand, in many practical situations, the geometry of the problem is too complex to allow the body–source coupling to be taken into account. In this case, the estimate of induced SAR neglecting the body–source coupling can only offer an order of magnitude accuracy, and a reliable estimate of induced SAR should be verified by experimentation.

## References

[1] K. M. Chen, "Interaction of electromagnetic fields with biological bodies," in *Research Topics in Electromagnetic Wave Theory*, J. A. Kong, Ed. New York: Wiley, 1981, ch. 13, pp. 290–347.

[2] O. P. Gandhi, "State of the knowledge for electromagnetic absorbed dose in man and animals," *Proc. IEEE*, vol. 68, pp. 24–32, 1980.

[3] C. H. Durney, "Electromagnetic dosimetry for models of humans and animals: A review of theoretical and numerical techniques," *Proc. IEEE*, vol. 68, pp. 33–40, 1980.

[4] D. Livesay and K. M. Chen, "Electromagnetic field induced inside arbitrarily shaped biological bodies," *IEEE Trans. Microwave Theory Tech.*, vol. MTT-22, pp. 1273–1280, Dec. 1974.

[5] I. Chatterjee, O. P. Gandhi, M. J. Hagman, and A. Riage, "Plane-wave spectrum approach for calculation of electromagnetic absorption under near-field exposure conditions," *Bioelectromagn.*, vol. I, no. 4, pp. 363–370, 1980.

[6] I. Chatterjee, M. J. Hagmann, and O. P. Gandhi, "Electromagnetic energy disposition in an inhomogeneous block model of man for near-field irradiation conditions," *IEEE Trans. Microwave Theory Tech.*, vol. MTT-28, pp. 1452–1459, 1980.

[7] A. Lakhtakia, M. F. Iskander, C. H. Durney, and H. Massoudi, "Near-field absorption in prolate spheroidal models of humans exposed to a small loop antenna of arbitrary orientation," *IEEE Trans. Microwave Theory Tech.*, vol. MTT-29, pp. 588–594, June 1981.

[8] M. F. Iskander, P. W. Barber, C. H. Durney, and H. Massoudi, "Near-field irradiation of prolate spheroidal models of humans," *IEEE Trans. Microwave Theory Tech.*, vol. MTT-28, pp. 801–807, 1980.

[9] A. Lakhtakia and M. Iskander, "Scattering and absorption characteristics of lossy dielectric objects exposed to the near fields of aperture sources," *IEEE Trans. Antennas Propagat.*, vol. AP-31, pp. 111–120, Jan. 1983.

[10] K. Karimullah, K. M. Chen, and D. P. Nyquist, "Electromagnetic coupling between a thin-wire antenna and a neighboring biological body: Theory and experiment," *IEEE Trans. Microwave Theory Tech.*, vol. MTT-28, pp. 1218–1225, Nov. 1980.

[11] J. Stratton, *Electromagnetic Theory*. New York: McGraw-Hill, 1941.

[12] S.-G. Zhu, K. M. Chen, and H.-R. Chuang, "Interaction of the near-zone fields of a slot on a conducting sphere with a dielectric sphere," NSF Tech. Rep., Michigan State Univ., 1983.

[13] S. Stein, "Addition theorems for spherical wave functions," *Quart. Appl. Math.*, vol. 19, no. 1, pp. 15–24, Apr. 1961.

[14] L. Infeld, "The factorization method," *Rev. Mod. Phys.*, vol. 23, no. 1, pp. 52–54, Jan. 1951.

[15] B. Friedman and J. Russek, "Addition theorem for spherical waves," *Quart. of Appl. Math.*, vol. 12, no. 1, 13–23, 1954.

[16] Y. Mushiake and R. E. Webster, "Radiation characteristics with power gain for slots on a sphere," *IRE Trans. Antennas Propagat.*, pp. 47–55, Jan. 1957.

**Shi-Guo Zhu** was born in Sichuan Province, China, in 1936. He graduated from the Electrical Engineering Department of Beijing Qing-Hua University in 1960. He then pursued advanced study in the fields of electromagnetics and fluid mechanics for two more years at the same university.

Since January of 1962, he has been teaching in the Physics Department of Sichuan University, China. In April of 1981, he came to the U.S. as a Visiting Scholar and participated in the research activity of the Electromagnetics Group in the Department of Electrical Engineering and Systems Science of Michigan State University, E. Lansing, MI. In the summer of 1983, he went back to China to rejoin the faculty of Sichuan University.

**Kun-Mu Chen** (SM'64–F'76) was born in Taipei, Taiwan, China, on February 3, 1933. He received the B.S.E.E. degree from the National Taiwan University, Taipei, Taiwan, in 1955, and the M.S. and Ph.D. degrees in applied physics from Harvard University, Cambridge, MA, in 1958 and 1960, respectively.

While at Harvard University, he held the C. T. Loo and the Gordon McKay Fellowships. From 1956 to 1957, he was a Teaching Assistant at the National Taiwan University, and from 1959 to 1960, he was a Research Assistant and Teaching Fellow at Harvard University. From 1960 to 1964, he was associated with the Radiation Laboratory, University of Michigan, Ann Arbor, where he was engaged in studies of electromagnetic theory and plasma. In 1962, while on leave from the University of Michigan, he was a Visiting Professor of Electronics at Chao-Tung University, Taiwan. Since 1964, he has been with Michigan State University, East Lansing, first as Associate Professor of Electrical Engineering, and since 1967, as Professor of Electrical Engineering. From 1968 to 1973, he was the Director of the Electrical Engineering program of the Department of Electrical Engineering and Systems Science. He has published numerous papers on electromagnetic radiation and scattering, plasmas, and the interaction of electromagnetic radiation with biological systems.

Dr. Chen is a fellow of the American Association for the Advancement of Science, a member of U.S. Commissions A, B, and C of the International Scientific Radio Union, Sigma Xi, Phi Kappa Phi, and Tau Beta Pi. He was the recipient of the Distinguished Faculty Award from Michigan State University, E. Lansing, in 1976. He was also the recipient of Excellent Achievement Award from Taiwanese American Foundation in 1983.

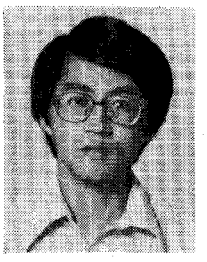

**Huey-Ru Chuang** (S'81) was born in Tainan, Taiwan, on August 18, 1955. He received the B.S. and M.S. degrees from the National Taiwan University in 1977 and 1981, both in electrical engineering. He worked on multibeam satellite antennas for his masters degree research. Currently, he is working toward the Ph.D. degree in electrical engineering at Michigan State University, E. Lansing, in the area of interaction of electromagnetic waves with biological bodies.

Mr. Chuang is a registered professional engineer in Taiwan.

# The Absence of Significant Short-Term Electromagnetic Bioeffects in Giant Algal Cells Exposed to CW and Pulse-Modulated *X*-Band Bursts

ASHOK V. GOKHALE, KATHLEEN MONTAIGNE BRUNKARD, AND WILLIAM F. PICKARD, SENIOR MEMBER, IEEE

***Abstract*—Giant cells of the algae *Chara brauni* and *Nitella flexilis* were exposed to continuous wave and pulse-modulated bursts of *X*-band microwaves and the vacuolar potential was monitored for immediate radiation-correlated offsets. No such offsets were observed despite a resolution of approximately 5 in $10^5$, and despite the wide variety of frequencies, power levels, and pulse protocols employed.**

## I. INTRODUCTION

THE BIOLOGICAL EFFECTS of nonionizing electromagnetic radiation now appear to be numerous and are being studied intensively (e.g., [1]–[4]). Those which seem to arise from direct electromagnetic heating of the test preparation (i.e., *thermal* effects) are generally the best characterized and least controversial. They tend to be associated with incident fields on the order of 100 W/m$^2$ (10 mW/cm$^2$) or greater. There are, however, in addition to putatively thermal effects, many others which, because of their occurrence at low power levels or because of the form of their variation with system parameters, can not readily be explained in ordinary thermal terms. These so-called *athermal* effects tend to be less well characterized and more controversial. They have been reviewed comprehensively by Adey [5].

Two characteristics common to most thermal and athermal phenomena are 1) a prolonged period of irradiation (at least minutes) is necessary for the effect to manifest itself and 2) the ability to resolve shifts in the vari-

Manuscript received October 12, 1983; revised March 7, 1984. This work was supported by the National Science Foundation under Grant ECS-8105485 and the office of Naval Research under Contract N00014-82-K-0261.

A. V. Gokhale and W. F. Pickard are with the Department of Electrical Engineering, Washington University, Saint Louis, MO 63130.

K. M. Brunkard is with the Department of Biology, East Stroudsburg University, East Stroudsburg, PA 18301.

0018-9480/84/0800-0795$01.00 ©1984 IEEE